analytical chemistry

ARTICLE

pubs.acs.org/ac

Technique Based on LED Multispectral Imaging and Multivariate Analysis for Monitoring the Conservation State of the Dead Sea Scrolls

Emilio Marengo,*[,†] Marcello Manfredi,[†] Orfeo Zerbinati,[†] Elisa Robotti,[†] Eleonora Mazzucco,[†] Fabio Gosetti,[†] Greg Bearman,[‡] Fenella France,[§] and Pnina Shor[⊥]

[†]Department of Environmental and Life Sciences, Università del Piemonte Orientale, Viale T. Michel 11, 15121 Alessandria, Italy

[‡]ANE Image, Consultant to the IAA for Imaging Technologies of the Dead Sea Scrolls, Pasadena, California, United States

[§]Preservation Research and Testing Division, Library of Congress, 101 Independence Avenue, SE, 20540 Washington, DC, United States

[⊥]Director of the Dead Sea Scrolls Digitization Project, Israel Antiquity Authority, Conservation Department, Rockefeller Museum, Post Office Box 586, Jerusalem, 91004, Israel

ABSTRACT: The aim of this project is the development of a noninvasive technique based on LED multispectral imaging (MSI) for monitoring the conservation state of the Dead Sea Scrolls (DSS) collection. It is well-known that changes in the parchment reflectance drive the transition of the scrolls from legible to illegible. Capitalizing on this fact, we will use spectral imaging to detect changes in the reflectance before they become visible to the human eye. The technique uses multivariate analysis and statistical process control theory. The present study was carried out on a "sample" parchment of calfskin. The monitoring of the surface of a commercial modern parchment aged consecutively for 2 h and 6 h at 80 °C and 50% relative humidity (ASTM) was performed at the Imaging Lab of the Library of Congress (Washington, DC, U.S.A.). MSI is here carried out in the vis−NIR range limited to 1 μm, with a number of bands of 13 and bandwidths that range from about 10 nm in UV to 40 nm in IR. Results showed that we could detect and locate changing pixels, on the basis of reflectance changes, after only a few "hours" of aging.

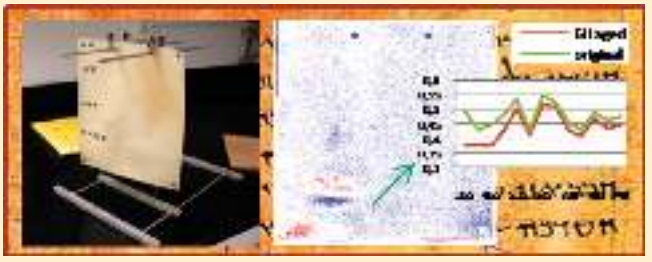

The discovery of the DSS some 60 years ago is considered to be one of the greatest archeological discoveries in modern times. The scrolls were written or copied in the Land of Israel between 250 BCE and 68 CE and were rediscovered in 1947 in 11 caves in the Judean Desert.[1] The Scrolls represent the oldest written record of the Hebrew Bible and contain the earliest copies of every book except Esther. This ancient library sheds insight into centuries of history that are pivotal to both Judaism and Christianity.

The conservation, preservation, and documentation of the DSS have concerned both scholars and conservators ever since their discovery. The constant and arid climate of the Dead Sea area, which is about 400 m below sea level, was probably the major factor in the preservation of these precious documents for over two millennia: removal of the fragile scrolls from the caves interrupted that environmental stability.

Since their discovery, the scrolls have been damaged by extreme environmental conditions (imbalance in humidity and temperature, excretions of animals, ...), and in the early years, by inappropriate conservation methods in a poorly controlled environment. About 80% of the scrolls are written on skin (from sheep and goats) and 20% on papyrus.[2−4]

The Israel Antiquities Authority (IAA) is Israel's state authority in charge of its archeological activities. In 1991 the IAA established a conservation laboratory dedicated solely to the DSS and has since been in the forefront in conservation techniques. The task of conservation and preservation of the scrolls is ongoing, because of their extreme brittleness and the need to make use of the most up-to-date conservation methods known.

The IAA has initiated a digitization project, both to monitor the well-being of the scrolls and to enable universal access while avoiding further damage to the scrolls, by creating high-quality images in color and infrared, and collecting multispectral data. With the assistance of Google-Israel, the IAA will support scholarship by creating and delivering to all who are interested the highest quality images of the DSS, coordinated with a new, usable integration of related scholarly resources, including transcriptions, translations, and bibliography.

The aim of conservation is to obviate damage caused by environmental or accidental factors. Materials of cultural property are

Received: April 27, 2011
Accepted: July 21, 2011
Published: July 21, 2011

subjected to changes over time due to the interaction with physical factors such as light, temperature, relative humidity, etc; chemical factors such as atmospheric oxygen, pollutants, etc.; and biological agents, including bacteria, fungi, insects, etc. Monitoring of the artifact over time can alert the conservator of potentially damaging situations. The objective of this research is to develop a monitoring methodology, using imaging, that not only does not damage the historical artifact, but also automatically recognizes areas (i.e., pixels) that are changing.

Modern imaging technologies have had a significant impact on archeology. Spectral imaging of manuscripts has been applied to improve the readability of documents and to assist in the assessment of their condition.[5] Spectral imaging with this imaging system acquires samples of the reflectance spectrum. The technique is well accepted in biology, medicine, atmospheric studies, marine ecology, and pollution control.[6−8] Caltech/NASA's Jet Propulsion Laboratory (JPL) has long been a leader in the application of this technology. Much research was originally conducted by remote sensing aircraft or orbiting spacecraft, but there is a considerable body of literature documenting its laboratory use for improving document legibility,[9] unscrambling palimpsests,[10] and analyzing the materials of paintings.[11,12]

Chemometric techniques (principal component analysis, classification methods, cluster analysis, etc.) have already been applied in the field of cultural heritage because they are able to extract systematic information from complex data sets.[13,14]

The theory of statistical process control (SPC)[15−18] can be used to investigate superficial degradation processes, as has previously been demonstrated by our group in monitoring the conservation state of wooden objects and canvas painted with inorganic pigments, analyzed by Raman and IR spectroscopy.[19,20]

This study proposes a new method, based on LED multispectral imaging coupled with multivariate analysis, for monitoring the state of the health of parchment surfaces. In the cases of the DSS and many papyri, spectral imaging has demonstrated that the reduction in visible contrast, and consequently the transition from legibility to illegibility, results from changes in the reflectance of the ink relative to the parchment (or papyrus) substrate.[21,22] Therefore, monitoring of the parchment reflectance suggests itself as a natural way to detect changes in the parchment. Our aim is to detect a degradation process of the parchment *before* its effects are visually recognizable, which indicates that significant damage has occurred. Advantages of our method include obtaining 39 MP (MegaPixel) images (dynamic range of 12 bits per channel, sensor array size of 49 × 37 mm), in about a minute with no thermal exposure to the object from lighting.

THEORY

Multivariate Statistical Process Control (SPC). Statistical process control is widely used in industrial applications but can also be advantageously applied to cultural heritage monitoring (Marengo, et al.[20]).

The general principle is to consider the conservation state as a process in its "in-control" condition, that is, when no deterioration effect is acting. Each further deviation from this initial condition is attributable to a damaging effect acting on the artistic object. The aim of this technique is automatic detection of a deterioration process in the substrate, as well as its localization and identification (i.e., which wavelengths are involved) before the human eye can detect the damage.

The multivariate approach is applied here to multispectral imaging that acquires samples of the reflectance spectrum for each pixel of the image. The resulting data set is a three-dimensional matrix in which the coordinates of pixels are on the x and y axes and the third dimension is the reflectance of each pixel at a defined wavelength, thus producing a "cube" of images.

Collecting a cube of images and using multivariate analysis allows the user to build control charts treating the object as a process to be monitored and controlled. The first step, as with implementing industrial process control, is to collect the data to build a training set to measure the system's natural variability, and the process is then monitored over time. If the natural variability of the imaging system is not correctly assessed at the outset, false/erroneous alarms or insufficiently sensitive charts will be obtained. The natural variability of a process includes all random oscillations that are expected to take place and that are not concerned with special and identifiable causes of variation. In this particular application, the natural variability could affect, for example, the LED power, wavelength and bandwidth, or camera resolution and sample illumination, providing slight and natural oscillations in the signal (absorbance) that is measured.

Principal Component Analysis (PCA). The data sets obtained using spectral imaging to study the conservation state of surfaces, are often characterized by large numbers of variables, with complex correlation patterns, due to the use of a spectral description of the surface.[23,24] In these cases, the application of a multivariate approach represents the best procedure for obtaining a rationalization of the data set. In the present study, PCA was applied to separate systematic information from experimental noise and random fluctuations. PCA provides a new set of orthogonal variables, linear combinations of the original ones, to describe the system under investigation in a compact and efficient way.

PCA can be applied to identify relevant changes caused by a degradation process, through the analysis of the projections (scores) of the original data (observations at different times) in the principal component (PC) space, while the analysis of the composition of each PC in terms of the contribution of the original variables (weights or loadings) may lead to the identification of the causes that produced the changes. Moreover, it is possible to calculate the information content of the residuals after extracting the relevant PCs. Normally, the residual matrix is expected to contain only noise and random fluctuations. In the present case, the residual matrix calculated from the image recorded after the degradation process has been applied may contain systematic information connected to the eventual presence of new species that were not present during the characterization step. Because these species were not present in that phase, they represent a new source of variation that probably is not accounted for by the PCs calculated on those data.[25−27]

Multivariate Shewhart Chart. Shewhart control charts are powerful tools for monitoring industrial processes and identifying the presence of assignable causes of variation.[15,16] When a process is described by a quantitative property, the corresponding Shewhart Control chart reports the behavior of the property along time. The region of statistical control is described as a range of values that lay within a range of values of $\pm 3\sigma$ around the average property value. This region corresponds to a confidence level of more than 99%. Anomalous process behaviors can be identified either when any point falls outside the $\pm 3\sigma$ region (α error is <1%) or when systematic trends are present. The upper control limit (UCL) and the lower control limit

(LCL) of this region are calculated using the following formulas:

$$\mathrm{UCL}_{\bar{\bar{x}}} = \bar{\bar{x}} + 3^{*}\mathrm{sd}(\bar{x})$$

$$\mathrm{LCL}_{\bar{\bar{x}}} = \bar{\bar{x}} - 3^{*}\mathrm{sd}(\bar{x})$$

when control charts are applied to pixel images, $\bar{\bar{x}}$ is substituted by $\bar{x}$ (the mean score of a pixel along a given PC calculated over some replications) and $\mathrm{sd}(\bar{x})$ is substituted by $\mathrm{sd}(x)$ (the standard deviation of the score of the pixel calculated over the replications).

In the present case, Shewhart control charts were constructed using the scores of the relevant PCs. In this way, if a sample violates the natural correlation structure characterizing the data set, this sample will show anomalous score values and will be recognized from their analysis.[28,29]

For the particular application to the monitoring of the conservation state, control charts can be effective tools: for pixel images collected along time, the presence on each image of pixels that violate the UCL or the LCL can be used to identify areas of the image where a significant damaging effect is present. The challenge is obviously the identification of such effects before they can be detected by the human eye to develop a method that allows a timely intervention.

PROCEDURE

The procedure developed for monitoring the conservation state of parchment consisted of the following steps:

(1) Imaging system setup. A preliminary study of the imaging system to identify the best instrumental conditions and the most sensitive operative parameters to be kept under control during the imaging sessions for the sake of data quality and reproducibility.

(2) Sample characterization. The sample's natural variability, including the natural variability of the imaging system (e.g., slight changes in LED power, wavelength and bandwidth, camera resolution, and sample illumination that produce slight differences in the signal that is measured when replications of the image are collected) must be evaluated and described. The description is accomplished by recording replicated images in multiple wavelengths (cubes) of the surface before application of any conservation. In our case, the baseline image cubes set the timeline to zero. The set of images obtained in this phase constitute the training set. The parchment in this phase can be considered "in statistical control" because no degradation process is active. The baseline cubes also are used to set the standard deviation of the data that serves as a classification parameter for the control charts. Naturally, the larger the variance of the baseline cubes, the less sensitive the method is. For this reason, we have spent considerable time on characterizing system stability and quantitative results. This method *explicitly* requires a stable and repeatable spectral imager that provides reliable quantitative results.

(3) Cube registration. Although the individual wavelength images for each cube are intrinsically registered, it is important that image cubes collected during different imaging sessions be registered.

(4) Unfolding cubes. The cubes are unfolded into a bidimensional matrix ($\mathbf{X}$) in which the columns are the 13 wavelengths and the rows are the pixels of the different images. The columns are mean-centered prior to any statistical analysis.

(5) Data set sampling. A good characterization of the in-control natural variability requires that several cubes be treated together so that a large amount of memory (several GBs) is necessary. A random sampling must preserve both the macro and micro information present in the cubes. The sampling was performed on the rows of the data matrix and provided a representative data set.

(6) Principal component analysis of the sampled baseline data set. This enables the description of the in-control situation natural variability by means of the relevant PCs that take into account the systematic relationships present in the data, example its covariance structure.

(7) Multivariate control chart. Multivariate Shewhart charts are calculated using the scores of the relevant PCs obtained in the characterization phase. In particular, from the training set data, it is possible to calculate the limits (UCL and LCL) that permit identification of the pixels that show anomalous behaviors along time.

(8) Parchment monitoring. The image of the parchment after application of temperature shock is aligned to the characterization images (see the Experimental Section for more details); the cube is then unfolded and centered using the mean calculated in the training session, and the new data are projected onto the PC space previously obtained. The scores of the new image are then compared with the LCL and UCL to identify which pixels' variance exceeds the control limits. Contribution plots, which show the contribution of each wavelength to the aging process for a defined pixel, enable us to determine which wavelengths are affected by degradation.

(9) Residuals analysis. As previously indicated, a further principal component analysis of the residuals matrix obtained after reprojection of the degradation images along the relevant PCs provides information on the eventual development of new sources of variation.

EXPERIMENTAL SECTION

LED Multispectral Imaging. We used a Eureka Vision LED system from MegaVision, Santa Barbara, CA, USA. The system has a 39-megapixel Kodak CCD monochrome sensor array, 49−37 mm, with 7216 × 5412 pixels, 6.8 × 6.8 μm, and two EurekaLight LED illumination panels. The camera produces images quantized to a dynamic range of 12 bits per channel. In this method, the spectral component is provided by fixed-wavelength light emitting diodes (LEDs) that emit in narrow spectral bands over ranges of wavelengths from the near-ultraviolet to the near-infrared. The LED bandwidth ranges from ∼10 nm in UV to 40 nm in the IR. The LED emissions are centered on the following wavelengths: 365, 450, 465, 505, 535, 592, 625, 638, 700, 735, 780, 870, and 940 nm. For principal component analysis, control charts and all other computations, we used the following: MATLAB (The MathWorks, version R2007b) and Photoshoot (version 4.0, MegaVision, CA, USA).

Our approach requires a well-characterized, quantitative system that returns absolute reflectance spectra, regardless of the imaging setup. Rather than relying on keeping everything the same for each imaging session, we simply measure the absolute reflectance accurately each time. We correct for illumination gradients, LED power variations and camera noise. The system

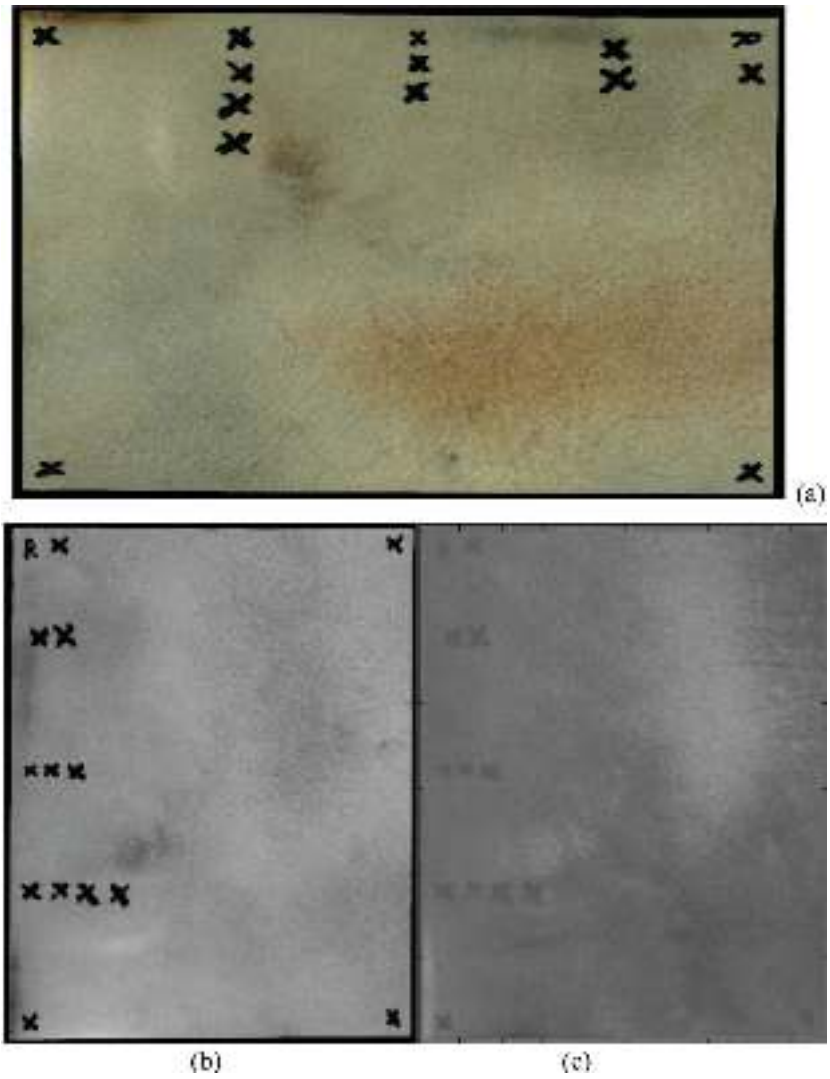

Figure 1. Color image of the parchment used in the present study (a) and projection of the score of the PC_1 (b) and PC_2 (c). In images b and c, pixels are represented on a gray scale: pixels with large negative scores are darker (toward black), and pixels with large positive scores are lighter (toward white).

performance and stability have been measured in several ways. One is retrospective, by happenstance: the system has been set up for imaging by MegaVision at three locations in the last year, and calibration images have been taken with color standard targets; in each case, we obtained the standard color space values and CIE spectral values to within a few percent. We also measured the LED performance-central wavelength, bandwidth and power, and modeled how those changes affected measured reflectance. All of these factors have negligible effect, and the system is very stable and reproducible. Results of the measurements and modeling have been reported in the literature.[30] The system has been extensively tested for thermal effects, and its data acquisition performance is well documented.[31,32]

Parchment. Parchment is a semitanned skin used as a writing surface in Asia Minor as far back as 200 BCE. Of all the components that make up living skin, only insoluble proteins (collagen) and water remain present in parchment. The proteins are grouped together, forming fibers of considerable physical consistency and excellent hydration capacity. Water is the only binding agent (fibers are joined together by means of hydrogen-bond bridges). The protein fibers are held together cohesively as long as the hygrometric balance is not disrupted. This means that the role of water and, more specifically, humidity, is of prime importance in the conservation of parchments.[33−35] High humidity can degrade the parchment by hydrolysis of the collagen as well as by denaturizing. In the case of complete saturation with water, the excessive number of water molecules transform the fibers into aggravated gelatins; decomposition of the parchment will be further aggravated by the effect of hydrolysis.[36,37] Low humidity and elevated temperature can dry out the parchment, locking in any gelatinization of the surface as well as promoting shrinkage and tearing by differential contraction. The skin is flexible thanks to the natural disposal of its protein fibers, but when the hygrometric balance is lost due to lack of humidity, the skin becomes rigid; desiccation leads to isolation of the protein filaments (linking by means of hydrogen bonds is lost), and this separation reduces flexibility, promoting cracking, exfoliation and even disintegration of the support.

A new 15 cm × 20 cm calfskin parchment (Figure 1a) was used in the present study (Pergamena Parchment LLC, Montgomery, NY, USA). The parchment was marked using a special ink (carbon black, lamp black, Natural Pigments, Willits, CA, USA): 14 symbols

were painted on the page. The parchment was aged in a temperature and humidity-controlled oven model 9121 (PGC, Black Mountain, NC, USA).

Methodology and Image Registration. Image cubes were corrected for illumination gradients by dividing the image cube by a reference cube from imaging of a standard 18% gray reference card.

Due to system stability, we needed to take reference cubes only infrequently. The data were then corrected for dark noise, normalized to unit exposure time and unit illumination power, and converted to absolute reflectance. The latter is done with a known NIST traceable reflectance standard in the image. With this approach, variables such as location of the light panels, the camera height, the *f*-stop, etc., are corrected and calibrated out, thus reducing the burden on imaging. However, as noted above, bad quantitative results for reflectance will lead to bad results with this method.

Image registration (also called alignment) is the process of overlaying two or more images of the same scene taken at different times[19] and represents a very critical phase, influenced by the resolution of the camera and by the position of the sample with respect to the camera sensor.

The final goal here is the comparison of cubes of images of an object taken when no degradation effect is present ("in-control" condition) to cubes of images of the same object collected along time or after a degradation process has started. The technique therefore requires the pixel-to-pixel comparison of images of the same object, and the correct alignment of the images to be compared is a crucial point in the monitoring methodology. For what regards in-cube registration, the images collected at different wavelengths at the same time can be considered intrinsically aligned and aberration can be considered negligible.

For what regards instead the intercubes registration, this was achieved using a customized software that minimizes the sum of squared differences calculated pixel-by-pixel between the images to be aligned.

Binning reduces the effects of misregistration while still leaving a high-resolution image to interrogate for changes. Since physical alignment of the images is not a simple task, we are aligning them using software (each IFOV on the parchment is 40 μm). Aside from the issues with positioning an object to that resolution, the fragments have poorly defined edges where the parchment is torn or cut.

RESULTS AND DISCUSSION

The choice of instrumental conditions is important for obtaining high-quality spectral images. The resolution used for the imaging session was 599 dpi, the highest resolution available for the size; the pixel size at the artwork plane was 0.04 mm. There is no mosaicking because the camera is not provided with bayer filters.

The light exposure of each waveband depends on the reflectance of the sample in that band and must be set individually for each band. The exposure times were determined by the Photoshoot software to set the maximum signal at a specified percentage of the CCD well depth. This was chosen to be 75% for these samples, which provides adequate dynamic range without clipping the upper and lower bounds.

The increase in temperature of illuminated LEDs changes the central wavelength and bandwidth, although their small thermal mass ensures that the temperature difference relative to the much larger heat sink is rapidly reduced. The camera software allows insertion of a delay between turning on the LED and acquiring the image. We determined that a 100 ms delay was sufficient to allow the LEDs to thermalize and stabilize.[30]

Training Set. A set of multispectral images was recorded and used as a training set to characterize system variability for statistical control, that is, before any aging. This was achieved by replicating the multispectral imaging acquisition of the parchment surface. The effect of some operative factors, such as the location of the parchment, instrumental settings, time of day, and location of the LED panels, were tested to account for sources of variability that could affect the monitoring along time. These factors were intentionally varied during the characterization step: moving the parchment in different positions; switching the instruments on/off; changing the instrumental conditions and returning them to the original setting; simulating other imaging sessions during the characterization; recording the images at different times of day; moving the panels of LEDs and returning them to the original position. Thirty-three cubes were recorded in optimal instrumental conditions as previously defined.

Each field of view contained a 99% reflecting lambertian reflector (Spectralon) and mini-color checker by X-Rite post-processing normalization of the incident LED power and to provide absolute reflectance standards. The CIE spectral values of the X-Rite color checker were measured separately as part of the calibration program and provided references for creating high-fidelity images using the six visible bands. Each cube included 13 wavebands with 7216 × 5412 pixels and was flattened by dividing the cube images by the textured flat field in the Photoshoot software.

Monitoring: Deterioration of Parchment. The parchment was aged in a special oven, under controlled conditions, at 80 °C and 50% relative humidity, for 2 and 6 h. One hour after the degradation process was finished, the parchment was imaged under the same instrumental conditions used for characterization of the process. The parchment did not show changes detectable by the human eye. The first five principal components calculated using autoscaled characterization measurements account for approximately 96.43%, 2.79%, 0.28%, 0.15%, and 0.06% of original variance. The first two alone (PC_1 and PC_2, respectively) account for 99.22% of the variance of the image bands. PC_1 and PC_2 were considered the only two significant principal components. In the score plot of PC_2 vs PC_1 (Figure 2a) the pixels (the objects) are well separated along PC_1 in two clusters that represent the text (black pixels) and the background (white pixels). As expected, the first component explains the differences between text and background.

The differences observed in the score plot can be explained using the loading plot shown in Figure 2b. The first component accounts for the information of all the channels: all the channels, in fact, show a large positive weight on this PC. The second PC mainly accounts for the information of UV (450 and 465 nm channels with large negative weights) and of the last two IR channels (870 and 940 nm with large positive weights). This means that along PC_2, those pixels with large reflectance at infrared wavelengths will have positive scores while those with large reflectance in the ultraviolet region will have negative scores. PC_2 means there is a typical contrast effect between high and low wavelengths that exhibit opposite loadings: when the

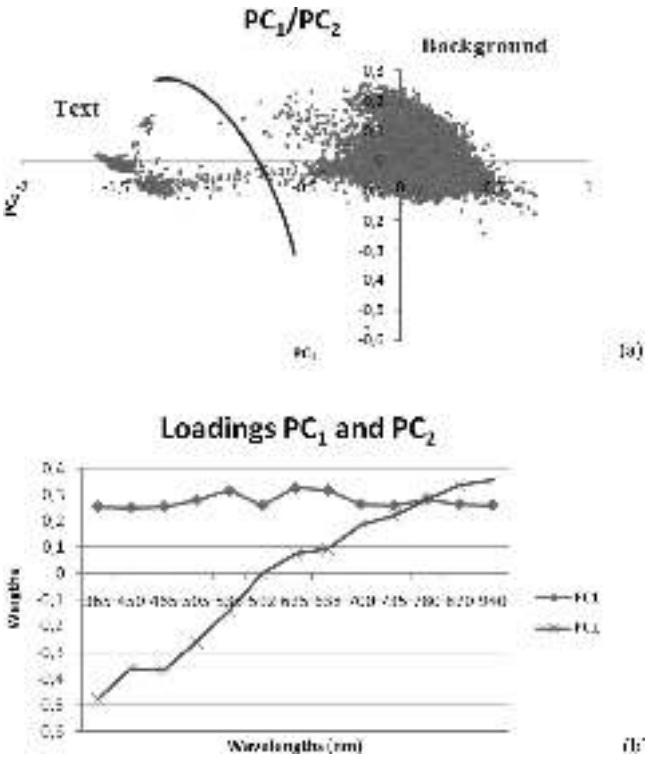

Figure 2. Score plot of PC_1 and PC_2 (a). The pixels are separated along PC_1 in two clusters that represent the text and the background. Loading plot of PC_1 and PC_2 (b): the first component accounts for the information of all channels together, and the second component mainly accounts for the information of UV and of the last two IR channels.

reflectance in the IR region increases, it decreases in the UV region and vice versa.

Each cube was projected onto the PC space using the loadings of the first and second PC; the result is a series of scores that compress the information from all 13 channels into two orthogonal channels (i.e., the first two PCs). The image obtained from the scores along PC_1 (Figure 1b) is very similar to the original image (Figure 1a), because only the differences related to pigmented and not pigmented areas are accounted for. So PC_1 acts as a filter and could be used also for increasing the document readability. In Figure 1c, the image is rebuilt using the information accounted for by PC_2.

The scores of the first PC of degraded parchment were compared with the UCL and LCL limits: Figure 3a and b shows the Shewhart control charts for PC_1 after 2 and 6 h aging, respectively. Each control chart is represented as an image in which the position of each pixel is rebuilt. Blue and red pixels in the charts are the out-of-control points of the parchment: blue pixels represent regions that exceed the LCL and red pixels are the regions that exceed the UCL. White pixels correspond to in-control points. The large number of red and blue pixels accounts for the general ability of the methodology to verify the existence of an aging effect. In fact, white pixels showing an in-control behavior are few. Considering the information accounted for by PC_1 (Figure 2b), blue pixels show a general decrease of the reflectance for all the 13 channels, and red pixels show the opposite behavior. Red and blue pixels are spread over all the image, but in some areas, they are grouped together to highlight entire regions (some of which are identified by circles in Figure 3). This behavior supports the conclusion on the ability of the method to identify damaged areas rather than providing false alarms (generally identified by scattered out-of-control pixels).

The two blue circles in the upper side of the charts represent the holes that were made, after the characterization, to put the parchment in the oven for the degradation. Wide areas of both images present values that exceed the LCL (indicated as blue circles on the image); this phenomenon is interpretable with a darkening of the parchment, not detectable by the human eye but recognized by the spectral imaging.

The contribution plots are represented in Figure 4; contribution plots allow in this case the identification of the wavelengths most responsible for the falling of a particular pixel out of the ULC or the LCL. They are calculated as the difference in that pixel between the original spectrum and the one after degradation; the difference is then multiplied by the loadings to identify the wavelengths responsible for the out-of-control event: wavelengths showing a large positive or negative contribution are the most responsible for the out-of-control. The contribution plot (Figure 4a) of the blue pixel ($x = 604$, $y = 880$) of the parchment shows that the first (365 nm, UV) and the 10th (735 nm, IR) channels are the main ones responsible for the out-of-control event; these two channels are the only two showing a large negative weight on the first PC. The absence of significant variations in the visible region (small positive or negative weights) explains why the human eyes cannot yet recognize it. In fact, the visible wavelengths (450, 465, 505, 535, 592, 625, and 638 nm) are less affected by the degradation process.

Some pixels that exceed the UCL are present in the control chart of Figure 3a and b; these pixels present a whitening effect. In particular, some areas with a diffuse presence of red pixels (identified by red circles) are present in the lower left corner of the charts aged 2 h. Here, two important regions that alternate blue and red pixels are present: in this part of the parchment, a cockle is present that formed during heating. The upper side of the cockle is the most exposed to the incident light, and it presents greater intensity values: the opposite is true on the opposite side of the cockle: in fact the lower side of the cockle is the dark area, and it is characterized by pixels that exceed the LCL values.

Figure 4c shows a contribution plot of a typical out-of-control ink pixel ($x = 150$, $y = 200$). The contribution plot shows that the degradation of the ink exceeds that of the parchment: the visible blue and green bands (λ = 450, 465, 505, 535 nm) and the infrared band at λ = 735 nm appear to be the principal ones responsible for the changes since they show the largest positive weights. Figure 4b and d shows contribution plots of parchment and inked pixels ($x = 150$, $y = 200$) aged 6 h, which are out of control. The contribution plots show that the degradation is greater than at 2 h of aging: the absolute value of the contribution of each wavelength increases from 2 to 6 h of aging, and the number of wavebands involved by the aging effect increases, as well.

The charts based on the scores of PC_2 are shown in Figure 3c and d. Again, blue and red pixels in the charts indicate the points of the parchment in the degraded cubes beyond the UCL (red pixels) or below the LCL (blue pixels). Wide areas of the image contain values that exceed the UCL (one of them is identified by

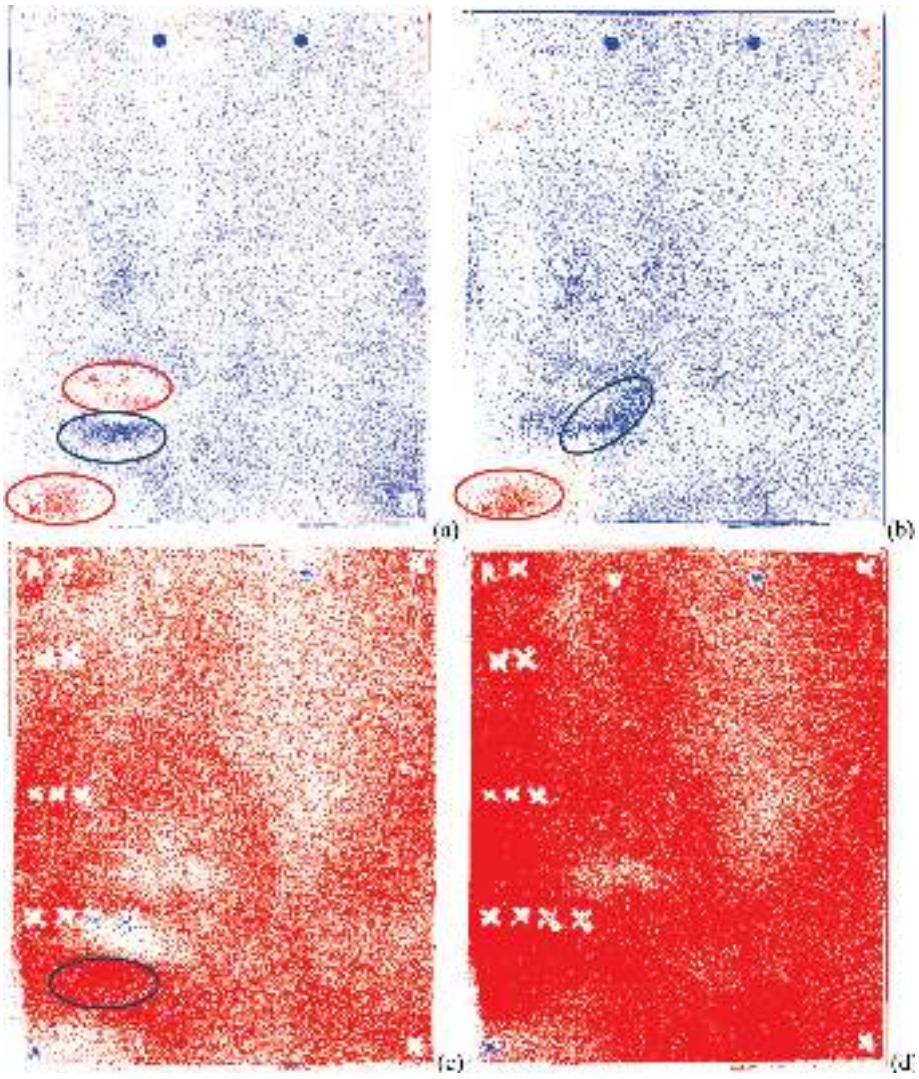

Figure 3. Control charts of PC_1 after 2 h (a) and 6 h of aging (b). Control charts of PC_2 after 2 h (c) and 6 h of aging (d). Blue and red pixels in the charts are the out-of-control points of the parchment: blue pixels represent regions that exceed the LCL and red pixels are the regions that exceed the UCL. White pixels show an in-control situation. Some of the widest out-of-control areas are identified by circles.

a blue circle). The contribution plots in Figure 4e and f of a red pixel at coordinates $x = 604$, $y = 880$ show that the first channel (λ = 365 nm) is the one primarily responsible for the out-of-control event, since it is characterized by the largest positive weight.

Figure 4g and h show the spectrum of original, 2 h, and 6 h aged ink and parchment. The reflectance of the ink spectrum progressively increases during the degradation process, and the reflectance of the parchment spectrum progressively decreases during the aging process. For the parchment, we see that the reflectance decreases with aging time in the oven, which is consistent with our notion that environmentally induced changes in the parchment decrease legibility by reducing reflectance. Why the ink also shows changes is unknown, perhaps because the very recently applied inks still contain binder and solutes that are continuing to evaporate as we age them. The inks on the scrolls do not contain such materials; though we cannot meaningfully compare the relative absolute reflectance of the inks on the scrolls, we do know that the ink spectra for both legible and illegible fragments are relatively flat, so it is the parchment reflectance that drives the ink contrast and, therefore, the legibility.

We also measured the L*a*b color coordinates for all image pixels using the X-Rite color checker as the standard. We created the transformation that converts gray values of the six visible bands to a high-fidelity color image in L*a*b color space. Using these values, we calculated the color difference between unaged and aged parchment using ΔE_{2000}, the standard color difference metric accepted by the International Commission on Illumination (CIE). We found that ΔE_{2000} between the original and the result of 2 and 6 h of aging were 1.18 and 1.69, respectively. A ΔE_{2000} of less than 2 is typically considered not perceptible by the human eye, so we are, indeed, detecting changes before they are visible.

Principal Component Analysis of the Residuals of the Degradation Analyses. To further investigate the effects of the applied aging treatment, a new PCA was performed on the residuals data matrix obtained by subtracting the information accounted for by the first two PCs of unaged parchment from the degraded image. The resulting residuals contain the information

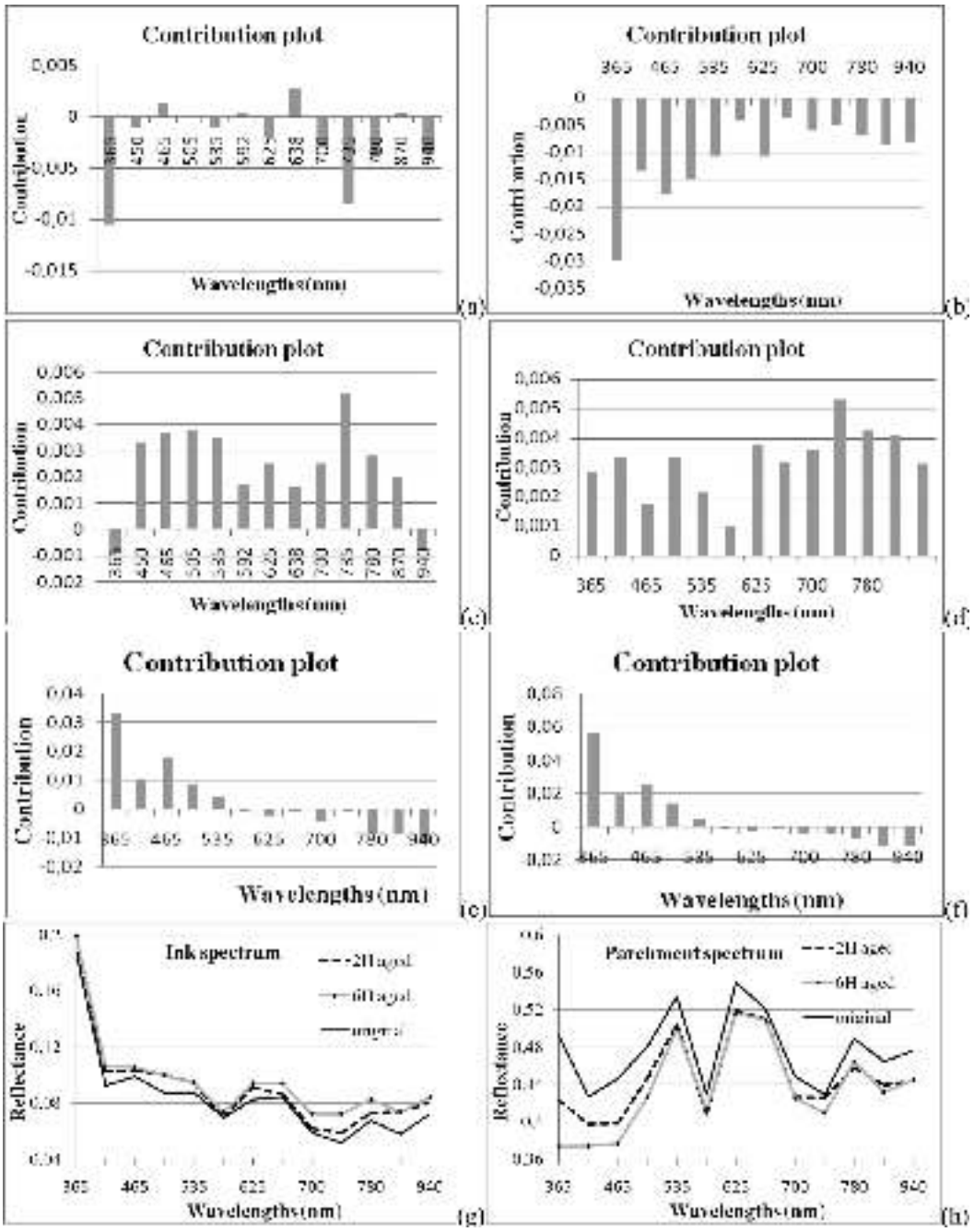

Figure 4. Contribution plots for PC_1 of the pixel $x = 604$ and $y = 880$ (belonging to the parchment) aged 2 h (a) and 6 h (b): the first and the 10th channels are the major ones responsible for the out-of-control event of the parchment pixels, since they show the largest contribution as an absolute value. Contribution plots for PC_1 of pixel $x = 150$ and $y = 200$ (belonging to ink) aged 2 h (c) and 6 h (d): the visible bands in the blue and green (450, 465, 505, 535 nm) and the infrared band at λ=735 nm appear to be the principal ones responsible for the changes in the ink pixels (largest contribution as an absolute value). Contribution plot for PC_2 of the pixel $x = 604$ and $y = 880$ (belonging to parchment) aged 2 h (e) and 6 h (f): the first channel (λ = 365 nm) is the principal one responsible for the out-of-control event (largest absolute contribution). Original, 2, and 6 h aged ink (g) and parchment (h) spectra. In general, the absolute value of the contribution of each wavelength increases from 2 to 6 h of aging, as shown by the spectra.

regarding formation of new species or events on the parchment surface that are not accounted for in the first two principal components of the unaged parchment. The first principal component accounts for 60% of the original variance and was deemed the only relevant PC. This information is probably due to changes occurring on the pigment surface during the aging treatment. The UV channel suggests the potential formation of new compounds (Figure 5), since it shows by far the largest absolute loading.

Figure 6 reports the residuals represented as images for all 13 channels separately. For each channel, the upper image represents the residuals with the information accounted for by PC_1, and the bottom image represents the same residuals after the information about PC_1 has been subtracted. A pattern

dx.doi.org/10.1021/ac201068s |*Anal. Chem.* 2011, 83, 6609–6618

apparently due to the pigment may be recognized in the image of the PCA residuals of the unaged parchment (Figure 6, upper), which indicates that the residuals convey information about the aging process. No systematic pattern may be identified after subtracting PC_1 (Figure 6, lower), which appears to indicate that only PC_1 contains information about the aging treatment.

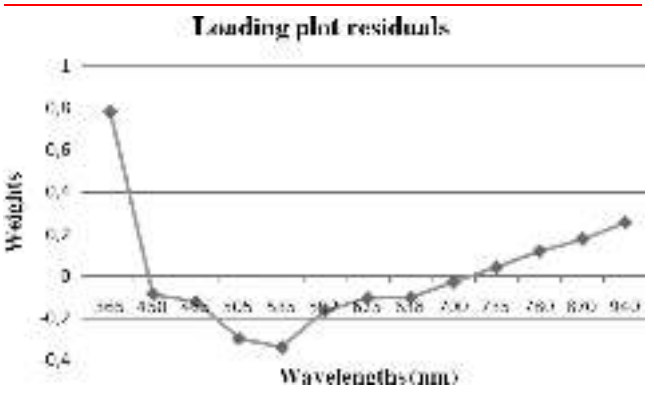

Figure 5. Loading plot of the residuals. The UV channel is the one mostly involved in the formation of new compounds or phenomena (it shows the largest absolute contribution).

CONCLUSIONS

The aim of this project is the development of a noninvasive technique based on LED multispectral imaging for monitoring the conservation of cultural heritage objects, particularly the Dead Sea Scrolls collection. The methodology here presented is developed and applied on a parchment model. The same methodology can be used for the next monitoring of the Dead Sea Scrolls.

A LED multispectral imaging system analyzed a sample of parchment before and after applying a degradation treatment. Multispectral imaging is carried out here in the vis-NIR range limited to 1 μm, with 13 channels of bandwidths ranging from ~10 nm in the UV to 40 nm in the IR. Our algorithms are able to detect degradation of the parchment before visually detectable damage has occurred. The chart also detects the presence of a cockle on the surface of the parchment that was generated by the heating in the oven. In addition, the method shows that the intensity of the spectra of out-of-control ink pixels increases and that the visible reflectance of the parchment decreases, as would be expected on the basis of the previous observation of ancient manuscripts. A future publication will consider artificial aging and degradation that is visible to the eye.

Out-of-control events may be interpreted from a contribution plot, and the channels responsible for the alarm may be isolated

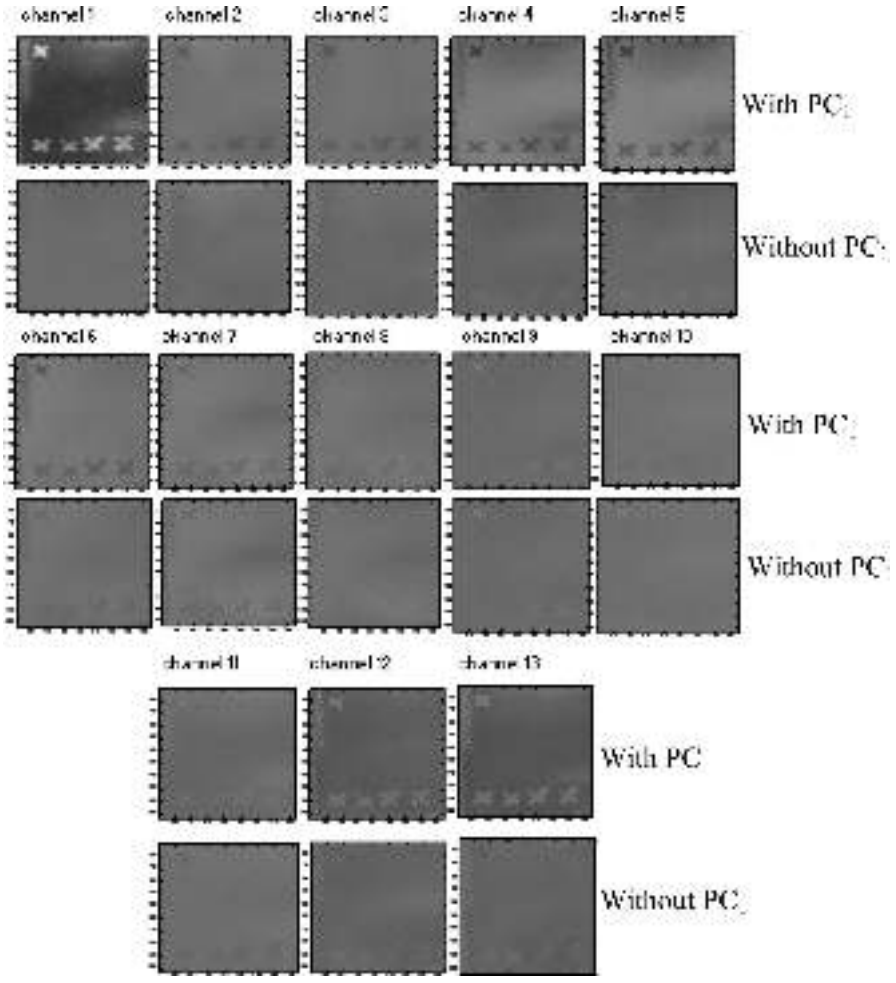

Figure 6. Residuals images of all 13 channels (up) and residuals images of all 13 images without the information accounted for by the PC_1 (down). No systematic pattern may be indentified after subtracting PC_1: PC_1 contains information about the aging process.

dx.doi.org/10.1021/ac201068s |*Anal. Chem.* 2011, 83, 6609–6618

and analyzed to interpret the chemical and physical processes that determine the event. The evolution of the damage during the degradation process may be detected from the control charts. Surface effects not accounted for by the initial PCA may be identified from a further PCA of the matrix of residuals. In other words, the PCA of the residuals may show spectral evidence of structural changes of the surface due to the aging treatment.

The proposed procedure is a pixel-by-pixel strategy, and it is dependent on image alignment, which is a crucial step in the algorithm workflow; this is the most critical step in the procedure. Our current images are aligned to one pixel with custom software. One pixel registration was achieved here and seems acceptable; less than a pixel registration can be achieved with centroiding.

Multispectral imaging was limited here to 1 μm in the IR region. Recently, it has been demonstrated that the IR region until 2.5 μm is very crucial in artwork analysis.[38,39] Actually, looking at higher wavelengths could be more effective; currently, however, the exploration of this spectral region can be envisaged only by the imaging system here described due to the lack of LEDs at wavelengths greater than 1 μm and also the lack of the corresponding sensors. Other imaging systems allow the exploration of such a spectral range, but they are more invasive to the sample since they are based on the use of standard lamps in the IR regions that may cause sample heating.

In conclusion, we affirm that the proposed approach may yield rapid and accurate measurements of the preservation state of manuscripts. The technique may be use also for other cultural heritage objects, such as frescoes and paintings. Obviously, due to the particular layering structure of such objects, a particular methodology of analysis and data treatment should be optimized. Industrial applications for the control of surfaces can also be envisaged.

AUTHOR INFORMATION

Corresponding Author

*Phone: +39 0131 360259. Fax: +39 0131 360250. E-mail: marengoe@tin.it.

ACKNOWLEDGMENT

This research is part of "The Dead Sea Scrolls Digitization Project", "The Leon Levy Dead Sea Scrolls Digital Library", of the Israel Antiquities Authority (IAA). The authors also acknowledge financial support from Regione Piemonte (Italy) (Project MEMIP-09).

REFERENCES

(1) Yadin, Y. *The Message of the Scrolls*; Simon and Schuster: New York, 1957; pp 161−162.
(2) Ryder, M. L. *Nature* **1958**, *182*, 781–783.
(3) Poole, J. B.; Reed, R. *Technol. Cult. III* **1962**, 1–26.
(4) De Vaux, R. *Archaeology and the Dead Sea Scrolls*; Oxford University Press: London, 1973.
(5) Knox, K. *Proc. SPIE* **2008**, *6810*, 681004–1-11.
(6) Carlotto, M. J.; Lazaroff, M. B.; Brennan, M. W. *124/SPIE* **1992**, 1819.
(7) Colarusso, P.; Kidder, L. H.; Levin, I. W.; Fraser, J. C.; Arens, J. F.; Lewis, E. N. *Appl. Spectrosc.* **1992**, *52*, 106A–120A.
(8) Paquit, V. C.; Tobin, K. W.; Price, J. R.; Mèriaudeau, F. *Opt. Express* **2009**, *17* (14), 11360–11365.
(9) Bearman, G. H.; Spiro, S. *Biblical Archaeol.* **1996**, *59*, 56–66.
(10) Easton, R.; Noel, W. *Gaz. Livre Médiév.* **2004**, *45*, 39–49.
(11) Delaney, J. K.; Zeibel, J. G.; Thoury, M.; Littleton, R.; Palmer, M. R.; Morales, K. M.; René de la Rie, R.; Hoenigswald, A. *Appl. Spectrosc.* **2010**, *64*, 584–594.
(12) France, F.; Christens-Barry, W.; Toth, M.; Boydston, K. *Proc. SPIE* **2010**, 7531.
(13) Bentley, J.; Schneider, T. J. *Comput. Statist. Data Anal.* **2000**, *32*, 465–483.
(14) Baronti, S.; Casini, A.; Lotti, F.; Porcinai, S. *Chem. Intell. Lab. Syst.* **1997**, *39*, 103–114.
(15) Shewart, W. A. *Economic Control of Quality of Manufactured Product*; Van Nostrand: Princeton, NJ; 1931.
(16) Montgomery, D. C. *Introduction to Statistical Quality Control*, 3rd ed.; Wiley: New York; 1991.
(17) Woodal, W. H.; Spitzner, D. J.; Montgomery, D. C.; Gupta, S. *J. Qual. Technol.* **2004**, *36* (3), 309–320.
(18) Pan, X.; Jarret, J. *J. Appl. Statist.* **2004**, *31* (4), 397–418.
(19) Marengo, E.; Robotti, E.; Liparota, M. C.; Gennaro, M. C. *Anal. Chem.* **2003**, *75* (20), 5567–5574.
(20) Marengo, E.; Robotti, E.; Liparota, M. C.; Gennaro, M. C. *Talanta* **2004**, *63*, 987–1002.
(21) Bearman, G.; Christens-Barry, W. A. *Palarch's J. Arch. Egypt/Egyptol.* **2009**, *6* (7), 1–20.
(22) Charbries, D.; Booras, S.; Bearman, G. *Antiquities* **2003**, 77.
(23) Pillai, K. C. S. In: *Encyclopedia of Statistical Science*; Kotz, S., Johnson, N. I., Eds.; Wiley: New York, 1983; Vol. 3; pp 668−673.
(24) Hotelling, H. In *Multivariate Quality Control-Techniques of Statistical Analysis*; Hastay, M. W., Wallis, W. A., Eds.; McGraw-Hill: New York, 1947.
(25) Vandeginste, B. G. M.; Massart, D. L.; Buydens, L. M. C.; Jong, S. D. E.; Lewi, P. J.; Smeyers-Verbeke, J. *Handbook of Chemometrics and Qualimetrics: Part B*; Elsevier: Amsterdam, 1998.
(26) Massart, D. L.; Vanderginste, B. G. M.; Deming, S. N.; Michotte, Y.; Kaufman, L.; *Chemometrics: A Textbook*; Elsevier: Amsterdam, 1988.
(27) MacGregor, J. F.; Kourti, T. *Contr. Eng. Pract.* **1995**, *3*, 403–414.
(28) Hayter, A. J.; Tsui, K. L. J. *Qual. Technol.* **1994**, *26*, 197–208.
(29) Wold, S.; Esbensen, K.; Geladi, P. *Chemom. Intell. Lab. Syst.* **1987**, *2*, 37–52.
(30) Bearman, G.; Christens-Barry, W.; Boydston, K. *Proc. Eikonopoiia*, Helsinki, Finland, 2010; pp 108−114.
(31) Christens-Barry, W. A.; Boydston, K.; Easton, R. L. *Proc. Eikonopoiia*, Helsinki, Finland, 2010; pp 27−38.
(32) France, F. G. *Proc. of Eikonopoiia*, Helsinki, Finland, 2010; pp 51−64.
(33) Reed, R. *The Nature and Making of Parchment*; Elmete Press: Leeds, 1975.
(34) Bykova, G. Z. *Restaurator* **1993**, *14* (3), 188–197.
(35) Hansen, E. F.; Lee, S.; Sobel, H. *J. Am. Inst. Conserv.* **1992**, *31* (3), 325–342.
(36) http://www.unesco.org/webworld/ramp/html/r8817e/r8817e00.htm#Contents. (Accessed February 8, 2011).
(37) Kathpalia, Y. P. *Conservation and Restoration of Archive Materials*; Paris, Unesco, 1973.
(38) Csèfalvayovà, L.; Strlić, M.; Karjalainen, H. *Anal. Chem.* **2011**, *83*, 5101–5106.
(39) Daffara, C.; Pampaloni, E.; Pezzati, L.; Barucci, M.; Fontana, R *Acc. Chem. Res.* **2010**, *43* (6), 847–856.